NSRRC-J04598 (2014)

APL MATERIALS 2, 113310 (2014)

Enhancement of surface enhanced Raman scattering activity of Au nanoparticles through the mesostructured metallic nanoparticle arrays

Shan-Chi Kuo,[1] Jin-Jia Tasi,[1] Jun-Sian Li,[1] Zheng-Hui Hou,[1] Cheng-Han Li,[1] U-Ser Jeng,[2] and Ying-Huang Lai[1,a]
[1]*Department of Chemistry, Tunghai University, Taichung 407, Taiwan*
[2]*National Synchrotron Radiation Research Center, Hsinchu Science Park, Hsinchu 300, Taiwan*

(Received 27 July 2014; accepted 12 October 2014; published online 23 October 2014)

A self-assembly template with a photoreduction agent embedded along mesostructured silicate-surfactant channels is prepared at the air-water interface. The unique template allows uniform and continuous uptake of metallic precursors into the silicate-surfactant channels from the solution subphase. Upon UV irradiation, the metallic precursors result in near-monodisperse nanoparticles homogeneously arrayed in the mesostructured polyoxometalated-silicate-surfactant (PSS) channels until saturation. With three dimensionally densely packed Au NPs of ca. 1.7 nm in the PSS template, hence a very high number density of surface-enhanced Raman scattering (SERS) hot-spots and large absorptive volume, we show that impressive SERS can be measured with 4-nitrothiophenol adsorbed to Au-NPs@PSS. © *2014 Author(s). All article content, except where otherwise noted, is licensed under a Creative Commons Attribution 3.0 Unported License.* [http://dx.doi.org/10.1063/1.4899116]

Mesomorphically patterned metallic nanoparticles (NPs) possess attractive properties for wide applications in, for example, microelectronics, molecular sensing, catalysis, and optoelectronics.[1–8] Especially in molecular sensing, the spacing and packing order of gold NPs were found to have an intriguing hotspot effect for drastically surface-enhanced Raman scattering (SERS).[9–11] In preparing such advanced materials, mesoporous silica with highly ordered channels provides convenient templates in formation and confinement of the size and distribution of metallic NPs reduced within the calcined channel pores.[12,13] Most of the syntheses of this type proceed in bulk solutions with dispersed metallic ions and reduction salts throughout silica channels and the solutions. Thus, reduced metallic NPs, however, block the channels to a certain extent, resulting in discrete NPs and trapped reduction agents inside the channels,[14–16] even less controlled is the contaminating formation of NPs outside the silica channels, leading to dispersed particle size and random distribution. In addition, closely and well dispersed Au NPs confined within the channels of template are the key to enhancing SERS because of the extreme SERS hot-spots effects.[13,17] Searching for a uniform reduction method to stuff mesopores with metallic NPs is of interest,[18–21] especially since mesostructured metallic NPs possess attractive properties for wide applications in microelectronics, molecular sensing, catalysis, and optoelectronics.[22,23]

Previous studies have demonstrated that meso-structured silica films synthesized at the air-water interface can exhibit highly oriented channel domains in large scale compared to that formed in bulk solutions.[24] Shown in an application, titania-surfactant composite films could be synthesized in one-step process at the air-solution interface by templating with a block copolymer surfactant from ethanolic solutions;[7] titania was, however, reduced from precursor ions for a matrix of

[a]Author to whom correspondence should be addressed. Electronic mail: yhlai@thu.edu.tw

 © Author(s) 2014

This article is copyrighted as indicated in the article. Reuse of AIP content is subject to the terms at: http://aplmaterials.aip.org/about/rights_and_permissions
Downloaded to IP: 140.110.200.41 On: Fri, 09 Jan 2015 01:23:01

limited meso-structure. With two successive reduction steps, metallic nanoparticles/nanowires were successfully grown inside silica films templated with block copolymers, SBA-15 or MCM 41;[9,13] discrete metallic NPs or short rods/wires inside the ordered Si channels were obtained. Using these hybrid materials as SERS substrates, SERS enhancement factors (EFs) as high as $\sim 10^3$–10^8 are obtained.[13,17,25] The degree of enhancement is found to depend on the number density of SERS hot-spots. Although one of the aforementioned studies observes the strongly enhanced due to the presence of ultrahigh density of hot-spots in Au-NPs@PSS,[17] to the best of our knowledge, studies on the adsorption behaviors of 4-nitrothiophenol (4-NTP) molecule on Au-NPs@PSS have not yet been performed.

In our previous study, we fabricated thin film shape ordered mesostructured polyoxometalate (POM)-silica composites containing Au NPs in the air-water interface. By anion exchange process, $AuCl_4^-$ ion was introduced to mesostructures and further reduced to Au metal by the photocatalytic reaction induced by POM.[17] In our designated synthesis route, the cationic-surfactant silica template with POM deployed on the surfaces of the 2D hexagonally packed channels is first prepared at the air-water interface, in which process, POM anions, such as $PW_{12}O_{40}^{3-}$ (PTA^{3-}), can partially intervene into the halide anions of the cationic surfactants, forming a hybrid photocatalytic, mesostructured silica (PSS) template. With metallic precursors introduced into the PSS template, metallic NPs can be reduced along the POM sites upon UV irradiation. Depending on the selected metallic precursors, NP arrays of various noble metals can be similarly prepared. Moreover, metallic NP arrays prepared with the PSS template can relieve from tedious purification process, as the template self-assembled at the air-water interface is largely free from the contamination of residual salts in the bulk solution. In this study, we demonstrate that metallic NPs can be directed and reduced along the pre-embedded POM (photocatalytic agents) on the channel surfaces of a cationic-surfactant-silica template; thereby, forming highly interconnected gold NPs of uniform particle size in the 2D hexagonally packed Si channels. With three dimensionally densely packed gold NPs of ca. 2 nm in the PSS template, hence a very high number density of SERS hot-spots and large absorptive volume, we also show that the impressive SERS can be measured with 4-NTP adsorbed to Au-NPs@PSS.

Fig. 1 illustrates the conceptual synthesis route for formation of patterned metallic NP arrays via the PSS template. Specifically, in an acidic environment of pH < 2.0, PTA^{3-} polyanions used can intervene partially into immobilized quaternary ammonium cations on the micelle interfaces owing to their comparable electrostatic interactions (compared to halide anions of the surfactants).[14] In the acidic solution, the introduced silicate precursors (S^+), here tetraethyl orthosilicate (TEOS), effectively adsorb to the complex charge-dipole shells (X^-I^+, with X^{-1} being either Br^- or PTA^{3-}) of the cationic micelles through a bridging counterion coupling for $S^+X^-I^+$;[15] the TEOS-$(PTA + Br)^-$-cetyl trimethylammonium (CTA^+) complex micelles of weakened charge interactions and reduced solubility, agglomerate and phase-separate to the air-water interface for a lyotropic film of hexagonally packed channels (i.e., the PSS template). With the introduction of metallic precursors, metal atoms can be reduced along the PTA sites of PSS upon UV irradiation and aggregate into metallic NPs in the soft organic phase of the silica channels.

In the typical synthesis, the PSS film was synthesized directly at the air-water interface from a sample solution containing the molar ratio PTA^{3-}/TEOS/CTAB (cetyl trimethylammonium bromide)/$HCl/H_2O = 3.9 \times 10^{-5}/0.28/0.10/1.6/100$, corresponding to a CTAB concentration of 2.0×10^{-2} M, at an ambient temperature within 2 h. Effect of photocatalyst concentration on the structures of the final product was studied by varying the quantity (0–8×10^{-6} M) of PTA. PSS films' lateral dimensions can be flexibly controlled by the dimensions of the reaction trough used. $AuCl_4^-$ (3×10^{-3} M, 20 ml) was introduced into the solution phase under the film. Adsorption of $AuCl_4^-$ to the PSS film at the air-water interface was evidenced by the feature changes of the UV-vis spectrum (Fig. 2), and the obvious film color change from pale to orange-yellow. No heat treatment for calcinations was needed. The $AuCl_4^-$@PSS film free floating at the air-water interface was directly subjected to UV irradiation for reduction of Au NPs. The final film of Au-NPs@PSS was then harvested from the air-water surface and was readily transferable to solid substrates (i.e., wafer or Kapton tapes) for further purification.

This article is copyrighted as indicated in the article. Reuse of AIP content is subject to the terms at: http://aplmaterials.aip.org/about/rights_and_permissions
Downloaded to IP: 140.110.200.41 On: Fri, 09 Jan 2015 01:23:01

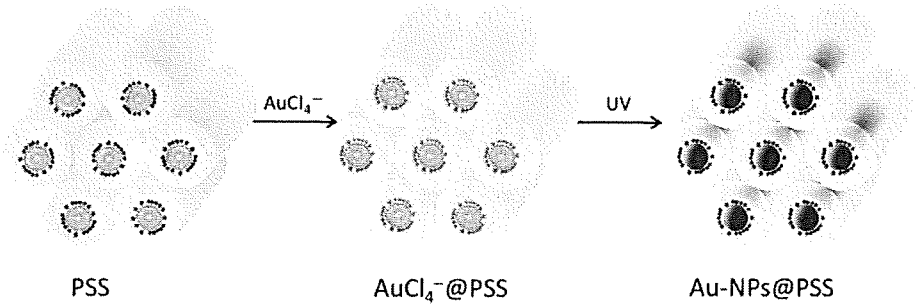

FIG. 1. Synthesis route for preparing 2D hexagonally patterned gold nanoparticle arrays via a cationic-surfactant silica template, embedded with photocatalytic agents PTA^{3-}.

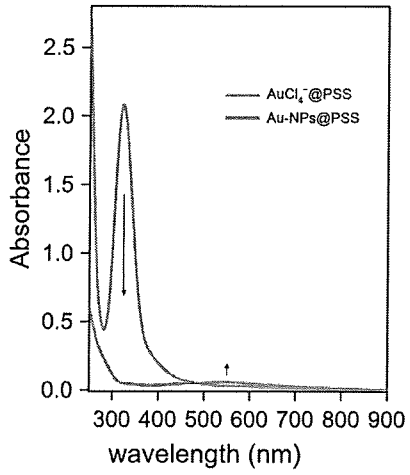

FIG. 2. UV-vis absorption spectra of the (a) $AuCl_4^-$@PSS (orange curve) and (b) Au-NPs@PSS (green curve).

Shown in Fig. 2 are the time-dependent UV-vis spectra measured for the $AuCl_4^-$@PSS film upon UV irradiation. The characteristic 320 nm absorption band of $AuCl_4^-$-CTA^+ complexes[11,26] decreased and diminished quickly within 5 min upon UV irradiation, implying efficient reduction of gold atoms via oxidation-reduction between $AuCl_4^-$ and isopropanol through photocatalytic agents during irradiation. Meanwhile, the absorption band near 550 nm gradually saturated within 3 h, signifying that gold atoms could aggregate into nanoparticles of similar sizes, presumably owing to the confinement of the mesostructured silicate channels of the template.

TEM examination was performed on a JEM-1010 microscope that was operated at an accelerating voltage of 200 kV. Specimens were prepared by ultrasonically suspending those PSS and Au-NPs@PSS in ethanol, applying the specimen to the copper grid, and drying in air. The TEM image taken for PSS template (Fig. 3(a)) exhibits highly oriented channels resembling that of uncalcined MCM-41.[2] This result suggests that PTA could be embedded successfully without deteriorating much the highly ordered silica channels of the cationic-surfactant-silica template. Moreover, Fig. 3(b) shows a TEM image taken for the Au-NPs@PSS film, exhibiting highly oriented channels with densely populated Au NPs.[17] The high resolution TEM (Fig. 3(c)) indicates that these Au NPs, of a rather well-defined size of ~1.7 nm, are packed closely and aligned along the silicate nanochannels for the highly oriented NP arrays. Had the gold NPs formed outside the channels, they would polydisperse in size and distribute randomly over the PSS template. The mean (center-to-center) spacing of the Au NP arrays estimated from the TEM image is ~3.2 nm (Fig. 3(c)), which matches closely with the channel spacing of the pure PSS template without loading of Au NPs. This further supports that Au NPs are well confined inside the silicate channels. X-ray energy-dispersive spectroscopy (EDS) reveals element signals of both silicon and gold throughout the Au-NPs@PSS film

This article is copyrighted as indicated in the article. Reuse of AIP content is subject to the terms at: http://apimaterials.aip.org/about/rights_and_permissions
Downloaded to IP: 140.110.200.41 On: Fri, 09 Jan 2015 01:23:01

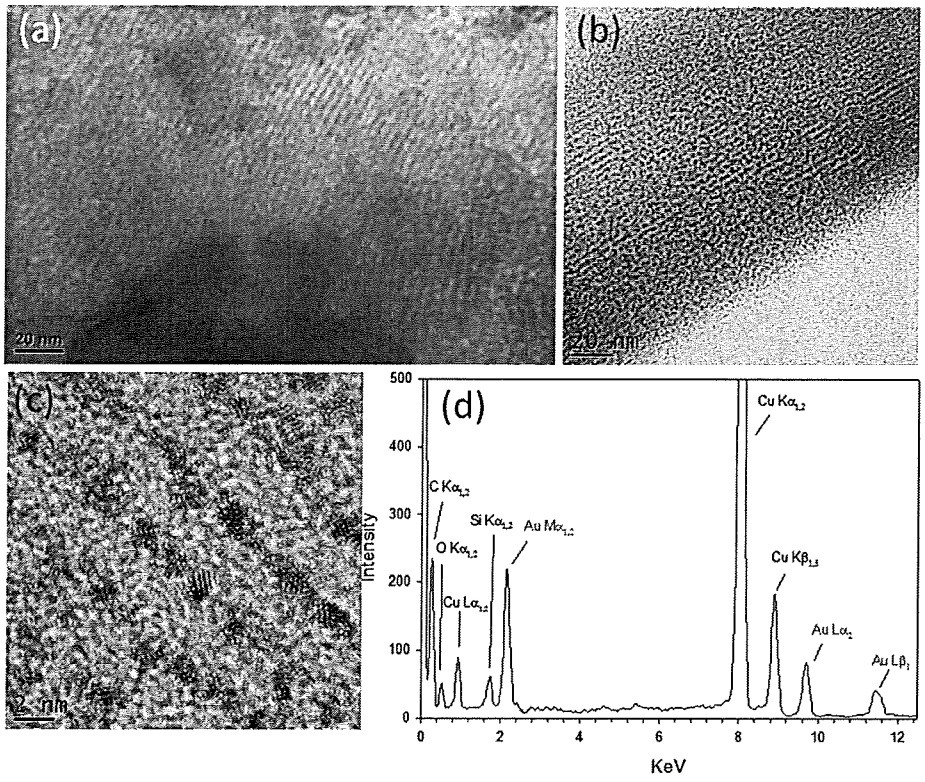

FIG. 3. (a) TEM images of the PSS template and (b) Au-NP@PSS. An HRTEM image of Au-NPs@PSS is shown in (c). The dark regions in (b) and (c) are Au NPs (globular or short rods) closely packed along the channels. (d) X-ray EDS coupled with TEM shows that both Si and Au elements exist throughout the Au-NPs@PSS composite.

(Fig. 3(d)). X-ray diffraction (XRD) result for the Au-NPs@PSS composite, as shown in Fig. 4, exhibits several broad humps corresponding to a face-centered-cubic (FCC) crystalline structure for crystalline Au NPs. The particle size 1.7 nm estimated from the XRD peak widths via the Scherrer equation is consistent with that observed from the TEM image.

The sample solution for GISAXS was prepared by adding TEOS into a surfactant solution of CTAB, with pH value <2. The mixture was then filled into a Teflon trough of an area of 80×80 mm^2 and a depth of 0.7 mm. The trough was further enclosed into an Al box with Kapton windows for GISAXS at an ambient temperature (~298 K). With a 10 keV beam (0.2 mm

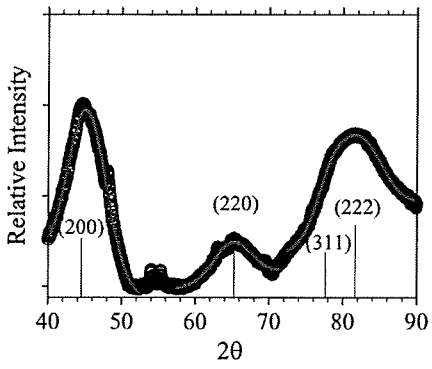

FIG. 4. XRD data for the Au-NPs@PSS film. The broad humps are indexed according to characteristic FCC reflections of gold crystallites.

This article is copyrighted as indicated in the article. Reuse of AIP content is subject to the terms at: http://aplmaterials.aip.org/about/rights_and_permissions
Downloaded to IP: 140.110.200.41 On: Fri, 09 Jan 2015 01:23:01

diameter) and a grazing incident angle of 0.15°, GISAXS data were collected using a Pilatus 1M-F area detector.[27] Shown in Fig. 5, is a representative 2D GISAXS pattern *in situ* observed from the air-water interface after the self-assembly of the PSS film. The GISAXS data in Fig. 5(a) reveal that the ordering peaks of the PSS template formed at the air-water interface of the sample solution are insensitive to the PTA concentrations ($0–8 \times 10^{-5}$ M) used. The fine spot-reflections could be completely indexed with 2D hexagonal packing (H), revealing that the PSS films comprising highly oriented H domains, with the channels oriented along the air-water interface.[6,14] The corresponding lattice size 4.24 nm is deduced from (10) reflection peak position.[6,15] The ordered domain size of the H domains estimated from the peak widths of the reflections was ca. 0.5 μm. Strikingly, the GISAXS pattern of PSS could be preserved remarkably well after loading of $HAuCl_4$ for *in situ* reduction of the Au-NP@PSS free floating film, as shown in Fig. 5(b); the enhanced peak intensities (attributing to Au NPs formation) together with the same peak position after UV irradiation strongly suggest a stable mesostructured template for formation and confinement of organized metallic NPs. The nearly same reflection positions and peak widths indicate the same H structure with a nearly identical H-lattice of $a = 4.19$ nm and similar ordered domain sizes. From the H-lattice size, a channel center-to-center spacing ($=2a/\sqrt{3}$) of 4.84 nm is deduced.[15] Compared to the mean channel d-spacing of 3.2 nm observed for the dried Au-NP@PSS film from the TEM image previously, the large d-spacing of the wet composite films at the air-water indicates a water layer of 1.6 nm between the silicate channels of the Au-NP@PSS film free floating at the air-water interface. Very likely, this water layer between silicate-surfactant channels plays a critical role in transporting $HAuCl_4$ into the PSS films for PTA site-directed photoreduction into gold atoms, which further aggregate into Au NPs and then deposit inside the silicate channels.

We note that in the acid condition of pH < 2.0, the binding of silicate precursors (S^+) to the complex charge-dipole shells (X^-I^+, with X^{-1} being either Br^- or PTA^{3-}) of the cationic micelles is through a weak bridging counter ion coupling for $S^+X^-I^+$. A previous report indicated that the Br^- anions could be replaced by Cl^- anions via anion exchange.[3] Reduction of nearly gold anion might result in a reduced charge repulsion of the surfactant head groups, hence a denser packing; this may allow some free space to accommodate (or confine the size) the Au-NPs in the channels.

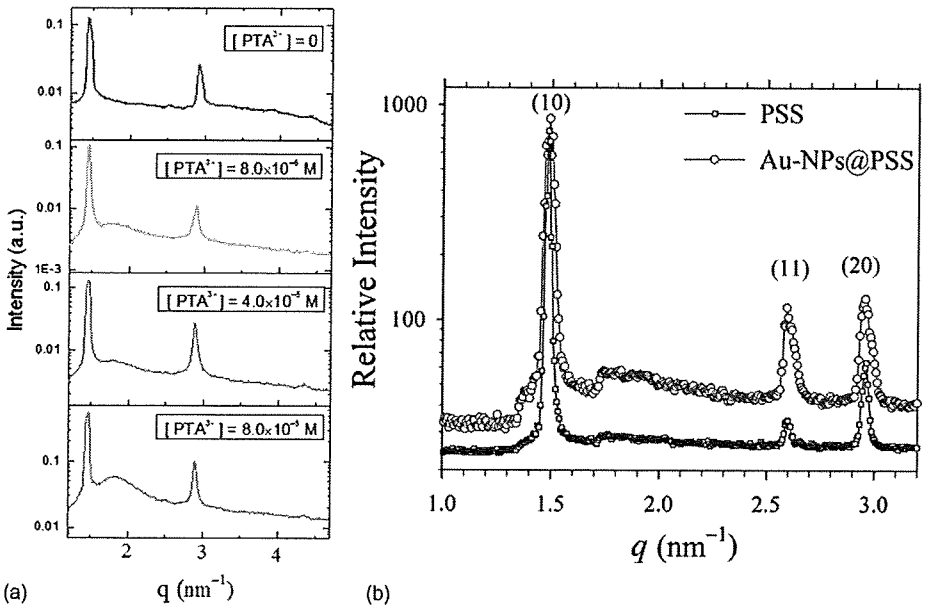

FIG. 5. (a) GISAXS data for the PSS templates prepared, respectively, at the air-water interface of the sample solution of TEO/CTAB/PTA, with the PTA^{3-} concentrations indicated. (b) GISAXS profiles of the PSS template and the subsequently formed Au-NPs@PSS film at the air water interface. The enhanced GISAXS peaks (indexed according to 2D hexagonal packing) in the latter case are attributed to enhanced scattering contrast upon formation of Au NP.

This article is copyrighted as indicated in the article. Reuse of AIP content is subject to the terms at: http://aplmaterials.aip.org/about/rights_and_permissions
Downloaded to IP: 140.110.200.41 On: Fri, 09 Jan 2015 01:23:01

To verify that Raman signal can be dramatically enhanced by placing the signal carrying molecules in the densely packed small Au NPs in Au-NPs@PSS composite, the SERS intensities of self-assembly of 4-NTP onto AuNPs@PSS are investigated. SERS samples were prepared by soaking Au-NPs@PSS composites (1.0 mg) in methanol solutions containing different concentrations (1 mM–10 nM, 1 ml) of 4-NTP for 18 h at an ambient temperature. After centrifugation, the samples were dispensed on glass slide substrate for SERS measurements. Raman scattering spectra were achieved by a home-built micro-Raman system. Samples were irradiated by He-Ne laser system (25 LHR/P 928, CVI Melles Griot) at 632.8 nm with output power up to 35 mW, focusing onto sample in diameter of 1 μm by a 40×/0.65 N.A. objective lens (Plan N, Olympus). The backscattered Raman signals from the sample were collected by the same objective lens, then passed into a monochromator (Shamrock 303i, Andor Technology) through a 632.82 nm ultrasteep long-pass edge filter (LP02-6332RE-25, Semrock) and were then detected by a cooled CCD camera (DU406, Andor Technology).The ruled grating (1200 l/mm) and the slit provided a spectral resolution of 5.5 cm^{-1} at blaze wavelength 500 nm. The laser exposure time was 10 s for each spectrum. Data were averaged from 6 spectra for improved statistics. Shown in Figure 6(a) is the prominent SERS spectrum of 4-NTP, with three sharp bands could be clearly observed even in the case with 10 nM 4-NTP solution. It is known that the SERS spectrum of 4-NTP is characterized by a prominent peak at 1078, 1336, and 1576 cm^{-1} corresponding to the stretching vibrations of C–S, N–O, and C–C, respectively.[28–30] The Stokes intensities of 4-NTP follow a Langmuir equation (Fig. 6(b)).[31] A saturated monolayer adsorption of 4-NTP is reached when the concentration of 4-NTP is >100 μM. At the same concentration, as shown in the Fig. 6(a), some features of 4-NTP are underneath the major peaks of 4-NTP. These SERS peaks of 4-NTP broadening agree well with the result of free and adsorbed 4-NTP coexistence. In accord with a previous SERS study,[17] we have estimated the SERS EF of the Au-NPs@PSS for the SERS bands using

$$EF = (I_{Au}/C_{Au})/(I_{ref}/C_{ref}), \quad (1)$$

where I_{Au} and I_{ref} are the corresponding band intensities of Au-NPs@PSS and PSS substrate after soaking in 4-NTP solutions of concentrations C_{Au} and C_{ref}, respectively. Compared to Raman spectrum for 4-NTP adsorbed to PSS substrate, the SERS of the 4-NTP/Au-NP sample with 10.0 nM 4-NTP concentration displays good EF values 3.0×10^5, 3.4×10^5, and 3.5×10^5, respectively, for the aforementioned three characteristic peaks. Quantitative SERS detection was obtained for Au-NPs@PSS with detection limits in the 10 nM concentration range.

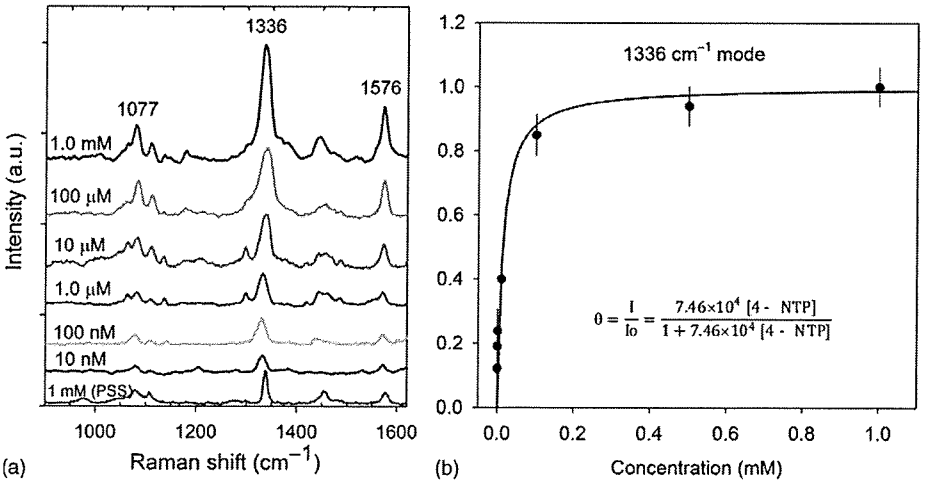

FIG. 6. (a) SERS spectra with 633 nm laser excitation for the Au-NPs@PSS composites 18 h after soaked in the 4-NTP solutions (with various concentrations: 1×10^{-3}–1×10^{-8} M). Also shown is the spectrum for a neat PSS film (without Au-NP loading) soaked in a 1 mM 4-NTP solution. (b) Adsorption isotherm of 4-NTP on the Au-NPs@PSS obtained according to 1336 cm^{-1} mode in the SERS spectra. I_0 is the peak intensity of a saturated 4-NTP monolayer.

This article is copyrighted as indicated in the article. Reuse of AIP content is subject to the terms at: http://aplmaterials.aip.org/about/rights_and_permissions
Downloaded to IP: 140.110.200.41 On: Fri, 09 Jan 2015 01:23:01

In summary, we have demonstrated that the mesostructured PSS template with phosphotungstic acids embedded along the channel surfaces of cationic-surfactant silica could self-assemble at the air-water interface. The PSS template formed is insensitive to the PTA concentrations ($<8 \times 10^{-5}$ M) used. Adsorption of chloroauric acid solution followed by UV irradiation leads to formation of gold NPs that can densely populate inside the channels for 2D hexagonally packed NP arrays. On the basis of the comprehensive SERS experiments, it is concluded that with narrow NP spacing gaps in three dimensions, Au-NPs@PSS composites exhibit prominent SERS effect. The corresponding 4-NTP detecting concentration limit is down to 10 nM, with corresponding SERS EF above 3×10^5. The Au-NPs@PSS exhibits a brilliant SERS performance, may have potential to be used as a SERS active substrate for molecular sensing with sieving.

The authors thank K.-F. Liao, C.-H. Su, and Y.-J. Chen for the assistance with GISAXS measurements, and Dr. Y.-C. Lee for the use of Raman spectrometer. This work was financially supported by the National Science Council and Ministry of Science and Technology (Grant Nos. NSC 102-2112-M-213-005-MY3 and MOST 103-2113-M-029-001).

[1] M. A. El-Sayed, Acc. Chem. Res. **34**(4), 257–264 (2001).
[2] T. Maschmeyer, F. Rey, G. Sankar, and J. M. Thomas, Nature **378**(6553), 159–162 (1995).
[3] K. Ariga, Y. Yamauchi, Q. Ji, Y. Yonamine, and J. P. Hill, APL Mater. **2**(3), 030701 (2014).
[4] L. Malfatti, D. Marongiu, S. Costacurta, P. Falcaro, H. Amenitsch, B. Marmiroli, G. Grenci, M. F. Casula, and P. Innocenzi, Chem. Mater. **22**(6), 2132–2137 (2010).
[5] L. Malfatti, P. Falcaro, B. Marmiroli, H. Amenitsch, M. Piccinini, A. Falqui, and P. Innocenzi, Nanoscale **3**(9), 3760–3766 (2011).
[6] M. D. Pérez, E. Otal, S. A. Bilmes, G. J. A. A. Soler-Illia, E. L. Crepaldi, D. Grosso, and C. Sanchez, Langmuir **20**(16), 6879–6886 (2004).
[7] M. C. Fuertes, M. Marchena, M. C. Marchi, A. Wolosiuk, and G. J. A. A. Soler-Illia, Small **5**(2), 272–280 (2009).
[8] E. D. Martínez, M. G. Bellino, and G. J. A. A. Soler-Illia, ACS Appl. Mater. Interfaces **1**(4), 746–749 (2009).
[9] L. Guerrini, E. Pazos, C. Penas, M. E. Vázquez, J. L. Mascareñas, and R. A. Alvarez-Puebla, J. Am. Chem. Soc. **135**(28), 10314–10317 (2013).
[10] J. Theiss, P. Pavaskar, P. M. Echternach, R. E. Muller, and S. B. Cronin, Nano Lett. **10**(8), 2749–2754 (2010).
[11] H. Ko, S. Singamaneni, and V. V. Tsukruk, Small **4**(10), 1576–1599 (2008).
[12] M. H. Nurmawati, P. K. Ajikumar, R. Renu, C. H. Sow, and S. Valiyaveettil, ACS Nano **2**(7), 1429–1436 (2008).
[13] Y. Zhu, D. Wang, L. Zhang, F. Sun, J. Xu, S. Jiang, and Q. Yu, RSC Adv. **3**(26), 10154–10157 (2013).
[14] M.-C. Liu, H.-S. Sheu, and S. Cheng, J. Am. Chem. Soc. **131**(11), 3998–4005 (2009).
[15] G. J. d. A. A. Soler-Illia, C. Sanchez, B. Lebeau, and J. Patarin, Chem. Rev. **102**(11), 4093–4138 (2002).
[16] L. Bois, F. Chassagneux, C. Desroches, Y. Battie, N. Destouches, N. Gilon, S. Parola, and O. Stéphan, Langmuir **26**(11), 8729–8736 (2010).
[17] Y.-H. Lai, S.-W. Chen, M. Hayashi, Y.-J. Shiu, C.-C. Huang, W.-T. Chuang, C.-J. Su, H.-C. Jeng, J.-W. Chang, Y.-C. Lee, A.-C. Su, C.-Y. Mou, and U. S. Jeng, Adv. Funct. Mater. **24**(17), 2544–2552 (2014).
[18] E. Yamamoto, M. Kitahara, T. Tsumura, and K. Kuroda, Chem. Mater. **26**(9), 2927–2933 (2014).
[19] J. Chen, Z. Xue, S. Feng, B. Tu, and D. Zhao, J. Colloid Interface Sci. **429**(0), 62–67 (2014).
[20] F. Chassagneux, L. Bois, J.-P. Simon, C. Desroches, and A. Brioude, J. Mater. Chem. **21**(32), 11947–11955 (2011).
[21] C. K. Tsung, W. B. Hong, Q. H. Shi, X. S. Kou, M. H. Yeung, J. F. Wang, and G. D. Stucky, Adv. Funct. Mater. **16**(17), 2225–2230 (2006).
[22] C.-J. Tsou, Y. Hung, and C.-Y. Mou, Microporous Mesoporous Mater. **190**(0), 181–188 (2014).
[23] F.-P. Chang, Y. Hung, J.-H. Chang, C.-H. Lin, and C.-Y. Mou, ACS Appl. Mater. Interfaces **6**(9), 6883–6890 (2014).
[24] H. Yang, N. Coombs, and G. A. Ozin, J. Mater. Chem. **8**(5), 1205–1211 (1998).
[25] R. Silva, A. V. Biradar, L. Fabris, and T. Asefa, J. Phys. Chem. C **115**(46), 22810–22817 (2011).
[26] K. Torigoe and K. Esumi, Langmuir **8**(1), 59–63 (1992).
[27] U. S. Jeng, C. H. Su, C.-J. Su, K.-F. Liao, W.-T. Chuang, Y.-H. Lai, J.-W. Chang, Y.-J. Chen, Y.-S. Huang, M.-T. Lee, K.-L. Yu, J.-M. Lin, D.-G. Liu, C.-F. Chang, C.-Y. Liu, C.-H. Chang, and K. S. Liang, J. Appl. Crystallogr. **43**, 110–121 (2010).
[28] W. Xie, B. Walkenfort, and S. Schlücker, J. Am. Chem. Soc. **135**(5), 1657–1660 (2012).
[29] X. Ren, E. Tan, X. Lang, T. You, L. Jiang, H. Zhang, P. Yin, and L. Guo, Phys. Chem. Chem. Phys. **15**(34), 14196–14201 (2013).
[30] H.-Y. Wu, Y.-H. Lai, M.-S. Hsieh, S.-D. Lin, Y.-C. Li, and T.-W. Lin, "Highly Intensified Surface Enhanced Raman Scattering through the Formation of p,p'-Dimercaptoazobenzene on Ag Nanoparticles/Graphene Oxide Nanocomposites," Adv. Mater. Interfaces (unpublished).
[31] H. Wang, C. S. Levin, and N. J. Halas, J. Am. Chem. Soc. **127**(43), 14992–14993 (2005).

This article is copyrighted as indicated in the article. Reuse of AIP content is subject to the terms at: http://aplmaterials.aip.org/about/rights_and_permissions
Downloaded to IP: 140.110.200.41 On: Fri, 09 Jan 2015 01:23:01